A Left-Handed α-Helix Containing Both L- and D-Amino Acids: The Solution Structure of the Antimicrobial Lipodepsipeptide Tolaasin

Fabrice Jourdan,[1] Silvia Lazzaroni,[2] Blanca López Méndez,[1] Pietro Lo Cantore,[3] Marianna de Julio,[1] Pietro Amodeo,[1] Nicola S. Iacobellis,[3] Antonio Evidente,[2] and Andrea Motta[1]*

[1]*Istituto di Chimica Biomolecolare del CNR, Comprensorio Olivetti, Pozzuoli, Napoli, Italy*
[2]*Dipartimento di Scienze del Suolo, della Pianta e dell'Ambiente, Università di Napoli Federico II, Portici, Italy*
[3]*Dipartimento di Biologia, Difesa e Biotecnologie Agro-Forestali, Università della Basilicata, Potenza, Italy*

ABSTRACT **The 18-amino acid cytolytic lipodepsipeptide tolaasin, produced in culture by virulent strains of *Pseudomonas tolaasii*, is the causal agent of the brown blotch disease of the cultivated mushroom. Tolaasin has a sequence of D-amino acids in its N-terminal region, then alternates L- and D-amino acids, and bears a C-terminal lactone macrocycle composed of 5-residues. The solution structure of tolaasin in sodium dodecyl sulfate was studied by 2D-NMR spectroscopy and molecular dynamics simulated annealing calculations. Tolaasin forms an amphipathic left-handed α-helix in the region DPro2-D*allo*Thr14 comprising the sequence of seven D-amino acids and the adjacent L-D-L-D-D-region. To the best of our knowledge, this is the first recognized example of a left-handed α-helix including both D- and L-amino acids. The lactone macrocycle adopts a "boat-like" conformation and is shifted from the helical axis as to form a "golf-club" overall conformation. These structural features will be of importance in understanding, and preventing, tolaasin's role in the bacterial colonization of the host plant, and its toxic action on cells. Furthermore, the observed antimicrobial activity together with the potential resistance to enzymatic degradation and the increased antigenicity (both due to the presence of L- and D-amino acids) strongly suggests for tolaasin a potential role as a template model for the design of new therapeutic antibacterial molecules. Proteins 2003;52:534–543.**

Key words: *Pseudomonas tolaasii*; *Agaricus bisporus*; antibiotic substances; amphipathic helix; SDS; NMR; molecular dynamics

INTRODUCTION

The emergence of antibiotic resistance in pathogenic bacteria has prompted a growing interest in antibacterial molecules that could serve as potential therapeutic drugs. One major group of targets includes polypeptides isolated from a variety of organisms, which fold into an amphipathic α-helical structure[1] upon association with lipid bilayers. Although the precise mechanism of the antibacterial activity is not yet fully understood, it has been suggested[2] that the target of these toxins is the cell membrane, whose permeability is increased through the formation of ion channels/pore via a "barrel-stave"[3] or a "carpet"-like manner[4] mechanism.

After the discovery that the insertion of D-amino acids into polypeptide sequences of L-amino acids confers a major resistance to enzymatic degradation and consequent inactivation,[5] and that short fragments containing D- and L-amino acids are of increased antigenicity,[6] several cytolytic peptides that incorporate D-amino acids have been investigated.[7,8] Polypeptides containing all D-amino acids (enantiomers of L-amino acids), having the tendency to fold into a helix, form a regular left-handed α-helix, and preserve the antibacterial activity.[5] The presence of only some D-amino acids dramatically reduces the α-helical structure of the peptides and, therefore, reduces their cytotoxic effects.[6] We demonstrate here that a limited number of L-amino acids can be incorporated into a left-handed α-helix without altering the regular structure, thus preserving the cytolytic properties.

Several phytopathogenic pseudomonads produce phytotoxic and antimicrobial lipodepsipeptides,[9] containing both L- and D-amino acids, that are classified in two groups according to their primary structures. The first group contains nonapeptides such as syringomycins, syringotoxins, syringostatins, and pseudomycins. The second group comprises syringopeptins, tolaasins, fuscopeptins, and corpeptins,[9] molecules from 18 to 25 amino acids, most of which have a D-stereochemistry.[10] The C-terminal region forms a lactone ring of 5 (tolaasins, fuscopeptins, and corpeptins) or 8 (syringopeptins) amino acids.

Grant sponsor: European Union; Grant number: ERBFM-RXCT960069.

This paper is dedicated to the memory of Prof. Guido Sodano.

Fabrice Jourdan, Silvia Lazzaroni, and Blanca López Méndez contributed equally to this work.

*Correspondence to: Andrea Motta, Istituto di Chimica Biomolecolare del CNR, Comprensorio Olivetti, Edificio 70, Via Campi Flegrei 34, I-80078 Pozzuoli, Napoli, Italy. E-mail: amotta@icmib.na.cnr.it

Received 27 March 2002; Accepted 3 January 2003

β-hydroxyoctanoyL-ΔBut1-DPro-DSer-DLeu-DVal5-DSer-DLeu-DVal-LVal-DGln10-LLeu-
DVal-ΔBut-D*allo*Thr-LIle15-LHse-DDab-LLys18
O ---------- C═O

Scheme 1. Tolaasin primary structure. The region forming the left-handed α-helix is underlined. A dashed line represents the lactone ring between D*allo*Thr14 and LLys18.

Tolaasin, a lipodepsipeptide produced in culture by virulent strains of *Pseudomonas tolaasii*,[11] is the causal agent of the brown blotch disease of the cultivated mushroom *Agaricus bisporus* (Lange) Imbach.[12–14] Its primary structure (Scheme 1) bears a β-OH octanoic acid blocking group at the N-terminus, a sequence of seven successive D-amino acids with a Ser-Leu-Val repeat in the N-terminal region of the peptide, and then alternate L- and D-amino acids. Tolaasin also contains some unusual amino acids, namely a Z-dehydroaminobutyric acid (ΔBut) at positions 1 and 13, a D-homoserine (Hse16), and a D-2,4-diaminobutyric acid (DDab17). Finally, a lactone ring is formed[13] between the hydroxyl of D*allo*Thr14 and the C-terminal LLys18.

Tolaasin has been shown to form Zn^{2+}-sensitive voltage-gated ion channels in planar lipid bilayers and to catalyze erythrocyte lysis by a colloid osmotic mechanism.[13,14] It exhibits many structural and functional similarities with alamethicin and it is possible that it may form ion channels in a similar manner. For alamethicin, aggregation of amphipathic α-helical monomers[15] appears to be the first step toward channel formation.[16,17] The observation that tolaasin biological action requires a minimal threshold concentration suggests a preliminary aggregation as the first step of channel formation.[18] An important feature of channel-forming peptides is that a bilayer surface appears to catalyze the α-helical conformation,[19,20] i.e., the peptide forms a stable amphipathic helix at the membrane surface. Accordingly, an amphipathic α-helix could be involved in the tolaasin channel formation mechanism.

To fully understand the molecular mechanism(s) of plasma membrane disruption by tolaasin, we studied its high-resolution structure in a membrane-like environment such as sodium dodecyl sulfate (SDS), which simulates the catalytic role of the membrane.[21] It was reported that in SDS, tolaasin exhibits a left-handed α-helical content of 20% calculated from circular dichroism (CD) spectra.[22] Such a percentage corresponds to one helix turn and does not even encompass the N-terminal sequence of 7 D-amino acids. Our 2D-NMR studies and molecular dynamics (MD) simulated annealing simulations show instead that in SDS, tolaasin assumes a left-handed α-helix in the region 2–14 thus including both D- and L-amino acids. This unusual finding appears to be the first example of a left-handed α-helix with both D- and L-amino acids. Furthermore, we confirmed that tolaasin inhibits the growth of Gram-positive bacteria, and also found that at low concentrations it is active against Gram-negative bacteria. Therefore, the presence of L-amino acids into the left-handed α-helix and the antibacterial activity suggest for tolaasin a potential role as a template for the design of new therapeutic antibacterial molecules.

MATERIALS AND METHODS

Bacteria Growth Condition

Type strain NCPPB2192 of *P. tolaasii* was grown on KB agar[23] at 25°C for 36 h, and then bacteria were suspended in distilled sterile water. One milliliter of the above suspension, containing about 108 colony-forming-units (cfu) mL^{-1}, was used to inoculate 500-mL Erlenmeyer flasks filled with 150 mL of liquid KB. Flasks were incubated under shaking (180 rpm) at 25°C for 48 h, and then cultures were centrifuged (12,000 rpm for 15 min); the resulting supernatants, if not processed for toxin purification, were lyophilized. The production in culture of tolaasin and the antimicrobial activity of the toxin preparations during the purification procedure were assessed by an antimicrobial assay[24,25] by using strain ITM100 of the Gram-positive bacterium *Bacillus megaterium* as a target microorganism.

Tolaasin Purification

Culture filtrate (1.350 L) was purified according to the reported method[26] opportunely modified as follows. The crude tolaasin precipitate (78.5 mg) was desalted by gel-filtration chromatography on Sephadex G-10 column (1.5 × 21 cm) eluted with distilled water (25 mL h^{-1}). The collected fractions (1 mL) were monitored by TLC, and the fractions containing tolaasin were combined and lyophilized to give a white solid residue. This procedure was applied three times, yielding a total of 42.3 mg of tolaasin. TLC analyses were carried out on silica gel plates (Merck, Kieselgel, 60 F 254, and 0.25 mm), and spots visualized by exposing the plates to UV radiation and spraying with 0.5% ninhydrin in Me_2CO. The ES and FAB MS spectra were recorded on a Perkin-Elmer API 100 LC-MS and a VG ZAB 2SE (Manchester, UK) spectrometers by direct injection and in a glycerol/thioglycerol matrix, respectively.

HPLC purification was achieved by injecting 1 mg of partially purified tolaasin, dissolved in 40% CH_3CN in 0.1% TFA, onto a semipreparative reverse phase C8 column (Brownlee Aquapore RP- 300, 1.0 × 25 cm); it was eluted with a gradient of 40% (v/v) to 52% (v/v) acetonitrile in 0.1% TFA over 25 min at a flow rate of 4.7 mL min^{-1}. The resulting tolaasin peak was collected, freeze-dried, and redissolved in HPLC grade ^1H_2O at an appropriate concentration prior to use.

Biological Assays

HPLC grade tolaasin was assayed for the antimicrobial activity against strains ITM100 and K12 ITM103, respectively, of *Bacillus megaterium* and *Escherichia coli*, and strain ATCC26423 of *Rhodotorula pilimanae*. Bacteria

were grown at 25 or 37°C for 48 h on nutrient agar containing 2% glycerol. Erlenmeyer flasks (500 mL), containing 200 mL of potato dextrose broth and placed on a rotary shaker at 180 rpm and 25°C for 72 h, were used for yeast growth. Ten-microliter drops of 1:1 serial dilution of a 128 $\mu g\ mL^{-1}$ toxin solution were spotted onto the plate agar surface containing 10 mL of potato dextrose agar. Toxin solutions containing 128, 64, 32, 16, 8, 4, 2, and 1 $\mu g\ mL^{-1}$ were used. After drops had dried, 500 μL of a suspension containing approximately 108 cfu mL^{-1} of the above-mentioned micro-organisms were added to 3 mL of soft agar (0.7%) and poured onto plates. After 48-h incubation at 25 or 37°C, the end serial dilution inhibiting the growth of the micro-organisms in the area of application of 10-μL solution, was recorded. The assay was repeated twice with three replicates.

NMR Sample Preparation

NMR samples of tolaasin were prepared by dissolving appropriate amounts of the peptide in 0.5×10^{-3} L of ^1H_2O, $C^2H_3O^1H$, DMSO-d_6, or $^1H_2O/^2H_2O$ (90/10 v/v) phosphate buffer, pH 7.0, in the presence of perdeuterated SDS at a concentration above the critical micelle concentration. The concentration of the lipodepsipeptide ranged from 0.92×10^{-4} M to 1.0×10^{-2} M.

NMR Spectroscopy

NMR spectra were recorded at 300 K on a Bruker DRX-500 spectrometer equipped with a triple resonance probehead and pulsed field gradients. Proton chemical shift assignments were performed using conventional two-dimensional (2D) experiments. Nuclear Overhauser enhancement spectroscopy (NOESY)[27] and total correlation spectroscopy (TOCSY)[28] experiments were recorded in the phase-sensitive mode with quadrature detection in ω_1 provided by the time-proportional phase incrementation scheme.[29] Water suppression was obtained by incorporating the WATERGATE sequence[30] in each experiment. Sixty-four transients of 2,048 points were collected for each of the 512 t_1 increments, with a spectral width of 6,024 Hz. Time-domain data matrices were all zero-filled in both dimensions to 4K, thus yielding a digital resolution of 2.94 Hz/point. NOESY experiments were obtained with mixing times of 0.10 and 0.25 s with no random variation. Clean versions[31] of the TOCSY experiments were recorded with spin-lock periods of 0.066 and 0.10 s, achieved with the MLEV-17 pulse sequence.[32] The gradient pulses were each 1 ms in duration and shaped to a sine envelope. Processing was performed using Aurelia 2.0 (Bruker Analytische) running on Silicon Graphics Indigo^2 R4400 computers.

Structure Calculations

Distance restraints were obtained from the 0.10-s mixing time NOESY spectrum recorded in $^1H_2O/^2H_2O$ (90/10 v/v) in the presence of SDS at 300 K. Volumes of NOE cross-peaks were integrated and calibrated with the AURELIA software. For intraresidual nuclear Overhauser effects (NOEs), we identified the allowed distance range from a dihedral systematic search by using the SANDER module of the AMBER 5.0 package.[33] A $\pm$ 0.01 nm tolerance was then allowed for each distance restraint. In the absence of stereospecific assignment for methyl and methylene protons, distance restraints were corrected for pseudoatom representation.[34] For methyl groups, an additional correction of 0.05 nm was added to take into account the multiplicity. The calculated distance restraints were used as upper limits for the structure calculations along with a general 0.18 nm lower distance limit.

The final interproton distance list comprised 299 upper limit distance restraints that were classified, according to Wüthrich,[35] into 77 intraresidue distances, 61 sequential interresidue restraints, 33 (i,i+1) distances involving at least one non-β sidechain proton, 96 medium-range interresidue distances relative to amino acids less than five positions apart in the sequence, and 32 [i,j ($|j-i|<5$)]. medium-range distances involving at least one non-β sidechain proton.

In vacuo structure calculations were performed by restrained simulated annealing (rSA) using a modified version of the Weiner et al. all-atom 1986 force field[36,37] containing a new set of parameters for ΔBut (López Méndez et al., unpublished data).

The starting structure was initially energy minimized to remove initial bad contacts, and then we performed five runs of rSA of 200 ps each (the time step was 0.001 ps). Each run was divided into 10 cycles of heating/cooling. During the cycles different high temperatures were reached (the highest one was 900 K). Berendsen's algorithm was used for heat-bath coupling with a time constant of 0.2 ps.[38] The SHAKE algorithm[39] was used to constrain all covalent bond lengths with a relative geometrical tolerance for coordinate resetting of 10^{-6} nm. The experimental restraints were gradually built up during the first 3 ps of each cycle of heating/cooling, and then were on for the rest of the cycle. The force constant for distance restraints was 8.33×10^3 kJ mol^{-1} nm^{-2}. Ten structures were selected within each run of rSA giving a total of 50 final rSA structures. All the 50 structures were successively refined by restrained energy minimization (rEM), and finally, the 20 lowest energy ones were selected to represent the 3D solution structure of tolaasin in water-SDS. In all the in vacuo calculations, we used a distance-dependent dielectric constant to roughly take into account solvation effects. A cut-off radius of 0.8 nm for nonbonded interactions with a standard residue-based pairlist routine was also used.

The lowest energy structure of tolaasin in vacuo was selected as the starting structure for the restrained MD (rMD) simulations in explicit solvent performed with AMBER 7 package,[33,40] and using the Particle Mesh Ewald (PME) methodology to compute long-range forces.[41–43] Pure methanol was the solvent of choice, because of unavailability of a reliable parametrization for SDS-water mixtures, and of by far longer equilibration times required by anisotropic, heavily charged mixtures of solvents including a large number of counterions. In our approach, restraints are responsible for introducing spe-

cific environmental effects, while methanol only represents a convenient way to provide a local environment capable to effectively solvate both polar and hydrophobic groups, thus avoiding computational artifacts of in vacuo simulations (exaggerated H-bonds, backbone-sidechain and/or end region interactions, lack of solvent-mediated long-range interactions).

The starting tolaasin structure for rMD was first neutralized with two chloride ions, and then a truncated octahedron box of methanol around the system was created. The closest distance between the wall of the box and the closest atom in the solute was 1.2 nm. The dimensions of the solvent box were 5.7 × 5.7 × 5.7 nm. In total, 1,870 methanol molecules were added.

Prior to MD simulation, the solvated system was initially minimized, constraining the solute atoms to their original positions with a force constant of 2.01×10^3 kJ mol^{-1} nm^{-2}. Then, in all 300 ps of equilibration MD simulations were carried out using the following protocol. Three cycles of 40 ps of restrained nVT MD with a gradual heating of the system from 0 to 300 K using the weak-coupling Berendsen's algorithm with a time constant for the heating bath coupling of 1.0 ps. Then, 90 ps of nPT MD with time constants for temperature and pressure coupling of 1.0 ps and 0.2 ps, respectively, and another 30 ps of nPT MD with the same time constant for heat bath coupling and rising the time constant for pressure coupling to 1.0 ps. During all these equilibration steps, the solute atoms were constrained to their original positions with a force constant of 2.01×10^3 kJ mol^{-1} nm^{-2}. The final 60 ps of equilibration MD were performed in the nVT ensemble with a time constant for heat bath coupling of 1.0 ps and gradually lowering the force constraint on the solute atoms. The time step was always 0.0015 ps.

After these equilibration procedures, the restrained nVT MD production run of 600 ps was started. It used the weak-coupling Berendsen's algorithm and a time constant for heat bath coupling of 1.0 ps. The time step for the production run was 0.001 ps.

In all MD simulations, the SHAKE algorithm was used to constrain covalent bonds involving hydrogen atoms with a relative geometrical tolerance for coordinate resetting of 10^{-6} nm. The force constant for distance restraints was always 8.33×10^3 kJ mol^{-1} nm^{-2}. For PME runs, the nonbonded cutoff value to limit direct space sum was 1.2 nm.

Ten periodically selected structures along the last 500-ps restrained MD are presented as representative of the MD results.

The molecular graphics program MOLMOL[44] was used to analyze and represent the 3D structures of tolaasin.

RESULTS

Secondary Structure Determination by NMR

NMR spectra of tolaasin were obtained in different solvents (^1H_2O, $C^2H_3O^1H$, DMSO-d_6, and aqueous SDS). Assignment of proton spin systems in all solvents used was obtained with the sequential methodology.[35] Tolaasin secondary structure was delineated from the qualitative pattern recognition approach of the sequential and medium-range NOEs as derived from 2D experiments. In ^1H_2O and $C^2H_3O^1H$, NOESY spectra essentially displayed sequential effects (data not shown), indicating that the conformation of the whole peptide was largely extended. In DMSO-d_6, proton chemical shifts were found to correspond to those previously reported.[13] NOESY spectra with 0.10 and 0.25 s mixing times showed some short- and medium-range NOEs in the region DSer3-DLeu7, simultaneously identifying tight turns as well as helical structure.[45] Most likely we are detecting an averaging between turns and helix, usually referred to as "nascent helix."[46] The rest of the peptide proved to be essentially extended.

The solution structure of tolaasin was then studied in a $^1H_2O/^2H_2O$ (90/10 v/v) solution in the presence of SDS at pH 7.0, a value at which the activity on erythrocytes is greatest.[18] The amide region of the NOESY spectrum at 0.10 s mixing time is shown in Figure 1. We observed sequential strong, non ambiguous NH_i-NH_{i+1} cross-peaks between all consecutive amino acids, with the only exception of the DGln10-LLeu11, LIle15-LHse16, LHse16-DDab17 NH_i-NH_{i+1} cross-peaks due to peak overlap. Furthermore, several NH_i-NH_{i+2} cross-peaks, namely DLeu4-DSer6, DVal8-DGln10, LLeu11-ΔBut13, DVal12-D*allo*Thr14 and LHse16-LLys18, were clearly observed. The presence of strong sequential NH_i-NH_{i+1} NOEs together with medium αCH_i-NH_{i+1} in the region DPro2-LVal9 is a first indication of a helical structure. This is confirmed by the observation of several medium-range NH_i-NH_{i+2}, αCH_i-NH_{i+2}, αCH_i-NH_{i+3}, αCH_i-NH_{i+4} and αCH_i-βCH_{i+3} NOEs. This NOE pattern, generally observed for right-handed helical structures in peptides and proteins with L-amino acids, suggests here the presence of a left-handed helix. The coexistence of αCH_i-NH_{i+2} and αCH_i-NH_{i+4} NOEs is generally more likely to occur within an α-helix.[35] From LVal9 to the C-terminal end of the depsipeptide, the presence of alternate L- and D-residues renders the NOE interpretation subtle. Observation of several medium-range effects (LHse16-LLys18 NH_i-NH_{i+2}, DGln10-DVal12 and DVal12-D*allo*Thr14 αCH_i-NH_{i+2}, DGln10-DBut13, DVal12-LIle15, and LIle15-LLys18 αCH_i-NH_{i+3}, DGln10-D*allo*Thr14 αCH_i-NH_{i+4}, and DGln10-DBut13, and DVal12-LIle15 αCH_i-βCH_{i+3}) suggests the presence of an ordered structure. However, it is important to underline that the standard distances observed for helices, β-sheets and turns in peptides and proteins containing only D- or L-residues cannot be used here to infer simply the folding of tolaasin in the region containing alternate D- and L- amino acids. Notwithstanding, the presence of key NOE effects between non-sequential residues of the same chirality (DGln10-DVal12, and DVal12-D*allo*Thr14 αCH_i-NH_{i+2}) hints at a turn-like folding.

In order to clarify the issue, we calculated the NOESY cross-peak intensities expected for a regular left-handed helix covering the 2–14 region, including the DPro2-DVal8 and the alternating L- and D- amino acids [Fig. 2(A)]. They were derived from the restrained minimized structure of a model-built depsipeptide imposing the dihedral angles ϕ and ψ to their expected values in a regular left-handed

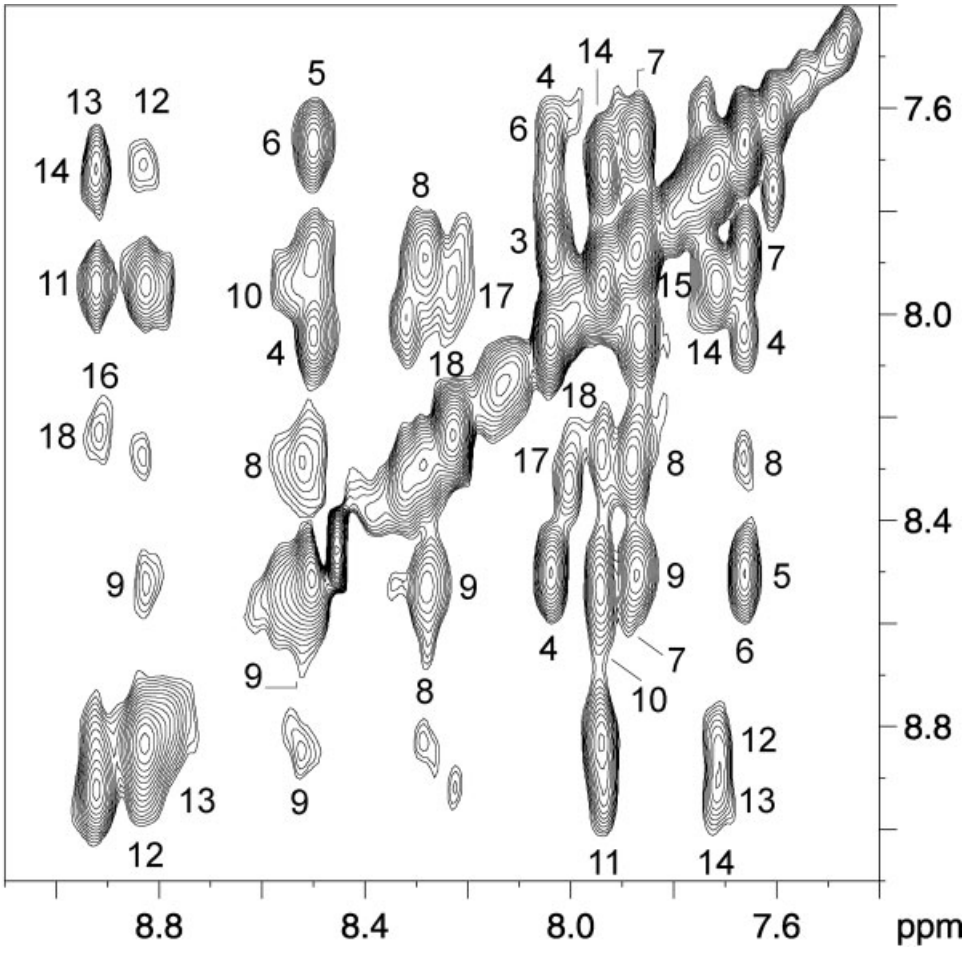

Fig. 1. NOESY spectrum of tolaasin in $^{1}H_2O/^{2}H_2O$ (90/10 v/v) in the presence of SDS with a mixing time of 0.10 s, 300 K, pH 7.0. Where space permits, the cross-peaks are labeled with the sequence number of amino acid residues.

helix ($\phi = +60$ and $\psi = +40$). As a comparison, we report the patterns of sequential and medium-range tolaasin NOEs [Fig. 2(B)], as obtained from the mean structure of the 20 lowest energy rSA/rEM tolaasin conformers (see below). All model interprotonic short distances [Fig. 2(A)] have a counterpart in either unambiguously assigned NOEs [Fig. 2(B), solid lines] or ambiguous/overlapped NOEs [Fig. 2(B), broken lines]. Such an agreement strongly supports the presence of a left-handed helix from DPro2 to D*allo*Thr14.

Three-Dimensional Structure Calculations

Three-dimensional structures of tolaasin were obtained using NOESY data collected from a 0.10-s mixing time NOESY spectrum in water-SDS and generated by a rSA/rEM protocol with the SANDER module of AMBER 5.0.[33] We carried out several runs of rSA calculations (for details see Materials and Methods section). Iterative back-assignment of ambiguous intra- and inter-subunit NOEs increased the number of experimental distance restraints from 269 to a final value of 299. The 50 structures obtained by the rSA protocol, with the final set of distance restraints, were refined by rEM, and the 20 ones with the lowest energy were chosen as representative of the 3D solution structure of tolaasin. The overall agreement among the 20 structures can be seen by the narrow range of energy distribution of the individual conformers (-821.7 kJ mol^{-1} ÷ -838.8 kJ mol^{-1}), and the low value of the root-mean square (RMS) deviation. The average RMS deviation for the backbone atoms of the whole depsipeptide is 0.036 ± 0.009 nm, and this value is reduced to 0.011 ± 0.004 nm when the better-defined region comprising residues 2–14 is considered. The statistics of NOE violations (Table I) demonstrates a good agreement with the experimental data. For all NOE types, the number of systematically violated NOEs in at least 50% of the 20 lowest energy rSA/rEM structures is $<15\%$ with larger NOE violations always <0.10 nm. A stereoview of the best fit superposition of the backbone atoms of the 20 rSA/rEM structures is shown in Figure 3(A). A unique fold is seen in the region 2–14 and described as a left-handed α-helix on the basis of dihedral angles ϕ and ψ values (Fig. 4). Typical regular left-handed helical values were found in the region DPro2-D*allo*Thr14, with RMS deviations $<12°$ for both ϕ and ψ.

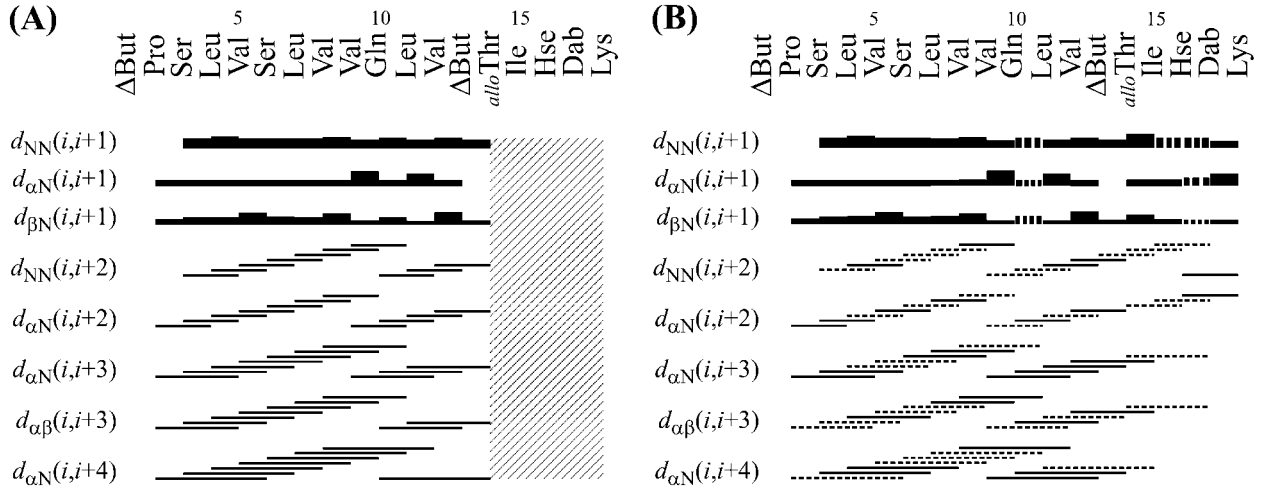

Fig. 2. Comparison between the sequential and medium-range NOESY cross-peaks of tolaasin folded in a standard left-handed α-helix (**A**), covering the 2-14 region, and those derived from the mean structure of the 20 lowest energy rSA/rEM tolaasin conformers (**B**). NOE intensities are indicated by the height of the bars. $d_{ab(i,j)}$ indicates the distance between the hydrogen atoms *a* and *b* located in the amino acid residues in the sequence positions *i* and *j*, respectively. In B, solid lines represent unambiguously assigned NOEs, while broken lines represent ambiguous or overlapping NOEs.

TABLE I. Analysis of the NMR Restraint Violations for the 20 Lowest Energy rSA/rEM Tolaasin Structures[†]

NOE type	NOE violations (%)	Max. violation (nm)
Intraresidue distances	3 (4.0)	< 0.02
Sequential interresidue restraints	8 (13)	< 0.03
(i,i + 1) distances involving at least one non-β sidechain proton	4 (12)	< 0.03
Medium-range interresidue distances	6 (6)	< 0.10
32 [i,j (|j-i| < 5)] medium-range distances involving at least one non-β sidechain proton	4 (12)	< 0.10

[†]In parentheses is shown the percentage of systematic NOE violations in at least 50% of the structures for each class of NOEs.

For LVal9 and LLeu11 a φ angular deviation (from 12 to 22, and from 7 to 23°, respectively), from the standard helical value was observed. However, the presence of a well conserved H-bond CO_i-NH_{i+4} pattern along the 2–14 region [Fig. 3(B)] warrants that these residues are in a helical conformation.

The backbone of the C-terminal cyclic region has a "boat-like" conformation and can be approximately described by an ellipsoid surface covering the backbone atoms of the ring [Fig. 3(B)], the angle between the helix axis and the largest axis of the ellipsoid ranging from 100.9° to 147.9° for the 20 lowest energy rSA/rEM tolaasin structures. Carbonyls of D*allo*Thr14, LIle15, and DDab17 and carbonyls of LHse16 and LLys18 point to opposite sides of the plane containing the ellipsoid surface. The side chain of LLys18 always spans out of the loop [Fig. 3(B)].

The lowest energy structure of tolaasin in vacuo was neutralized and solvated in a truncated octahedron box of 1,870 methanol molecules. rMD results confirm the rSA/rEM tolaasin structure as shown by the φ and ψ angle values and the angular order parameters (Table II) for 10 periodically sampled structures along the last 500 ps of rMD. φ and ψ angle values typical of a left-handed α-helix are observed from DPro2 to D*allo*Thr14 with corresponding high values of angular order parameters (>0.9) confirming the stability of the helical structure.

Analysis of the amino acid distribution within the helix highlights the amphipathic nature of the left-handed α-helix. Polar amino acids (DSer3, DSer6, and DGln10) lie on the same side of the α-helix [Fig. 5(A)]. Furthermore, the C-terminal lactone ring, showing a significant hydrophilic character due to residues LHse16, DDab17, and LLys18, is also located on the same side, thus creating a continuous surface from DSer3 up to the loop edge [Fig. 5(B)].

Spectrum of Activity

Apart from the major target of tolaasin, the disruption of plasma and vacuoles membranes rending the collapse of mushroom cells, other roles have been described. As a non host-specific toxin, tolaasin causes lysis of a range of cell types, including fungal, plant, and animal cells. The toxin has been reported to inhibit the growth of almost all-fungal and Gram-positive bacteria, and causes cytolysis and necrosis in various plants, though a different sensitivity among them is apparent.[18] We confirm that Gram-

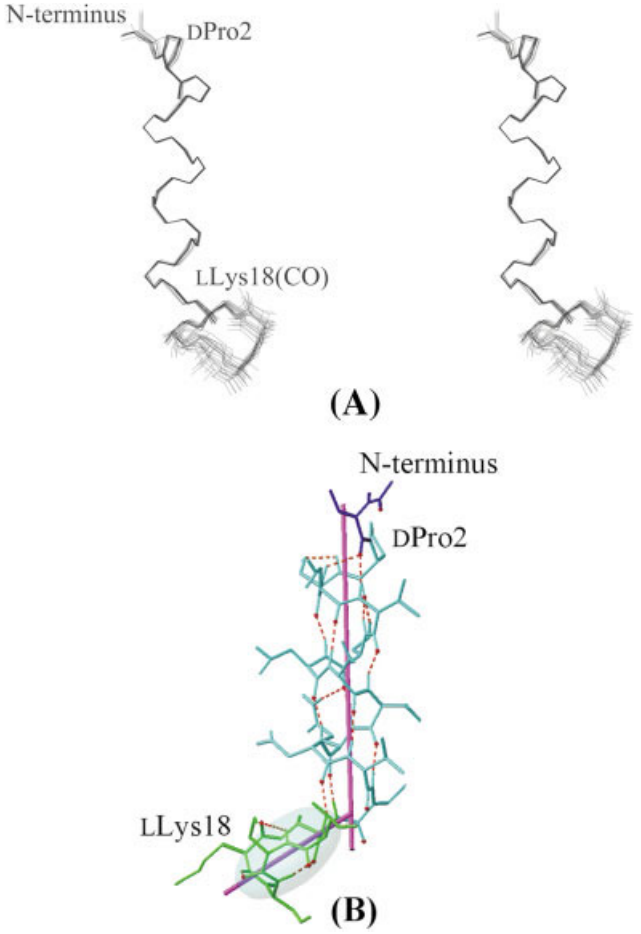

Fig. 3. Calculated structures of tolaasin. **A:** MOLMOL stereoview of the best-fit superposition of the 20 lowest energy rSA/rEM conformations of tolaasin. Backbone atoms of residues 2–14 were used for the best fit. **B:** Stick representation of the "golf-club" like tolaasin conformation. Dotted lines indicate hydrogen bonds along the left-handed α-helix. The helical axis inside the helix is also represented. The shaded area simulates the ellipsoid that covers most of the backbone atoms of the lactone ring, and its largest axis is also shown.

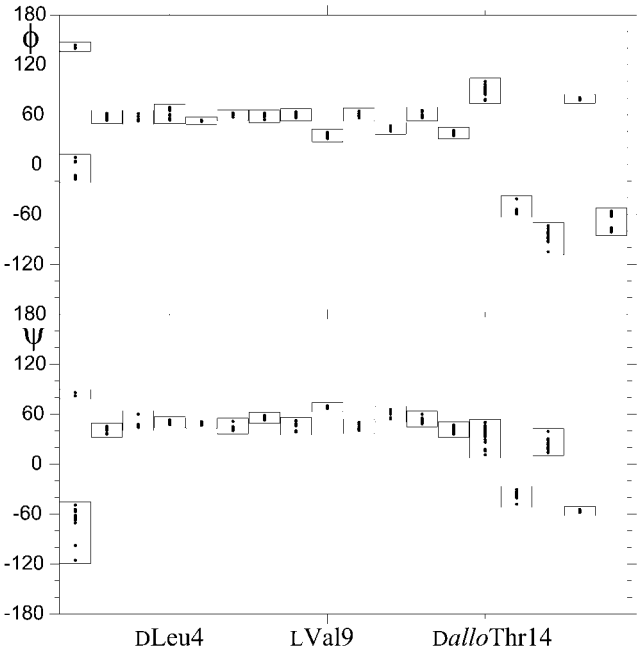

Fig. 4. ϕ and ψ distribution of 20 lowest energy rSA/rEM tolaasin conformations. Bars group angle values differing less than 30° from adjacent points.

positive bacteria are sensitive to low concentrations of tolaasin (for example, the growth of *B. megaterium* was inhibited by 4 μg mL^{-1} of tolaasin); however, a toxin concentration of 64 μg mL^{-1} also inhibited the growth of the Gram-negative bacteria *E. coli* and the yeast *R. pilimanae*. The results for Gram-negative bacteria are in contrast with the activity reported,[18] where it has been shown that such bacteria are sensitive to low concentrations of tolaasin but in the presence of an outer membrane perturbing agent such as polymyxin B.

DISCUSSION

In SDS micelles, tolaasin forms an amphipathic left-handed α-helix in the region DPro2-DThr14. It comprises a sequence of seven D-amino acids (DPro2-DSer-DLeu-DVal5-DSer-DLeu-DVal8) and a stretch of L- D- L- D- D- amino acid residues (LVal9-DGln-LLeu-DVal-ΔBut-D*allo*Thr14). To the best of our knowledge, this is the first recognized example of a naturally occurring molecule with a regular left-handed α-helix including both D- and L- amino acids, and it could be relevant for the de novo design of protein structure. As a comparison, the closely related lipodepsipeptide syringopeptin 25-A also forms a left-handed α-helix, but only includes residues of D- chirality.[47] A percentage of 20% left-handed α-helix has been calculated from CD data, and it was hypothesized that the helix could be located in the N-terminal sequence of 7 D-amino acids.[22] However, the CD data do not allow to specifically position the helix in the sequence as 20% of the sequence represents only 3.6 residues, i.e., a single helix turn.

The C-terminal lactone loop adopts a "boat-like" conformation and is found shifted from the helical axis; therefore, tolaasin assumes a "golf-club" conformation [Fig. 3(B)]. It has been reported that in polymixyns,[48] ranalexin,[49] and in type-I brevinins,[50] the cationic heptapeptide ring is responsible for the disruption of bacterial membrane permeability and thus for antibiotic activity. The octapeptide lactone ring of syringopeptins also shows two positively charged residues in identical positions to those of the above molecules.[47] Identically, in tolaasin two positively charged groups (DDab17 and LLys18) are found in the pentapeptidic C-terminal lactone ring. This finding could imply that, independently from the size of the ring, the presence of positive charges into the loop, together with the amphipathic helix, could represent a fundamental membrane-permeabilizing motif.[51,52]

It has been reported that tolaasin is able to provoke hemolysis on horse erythrocytes, and that it results from the formation of pores in erythrocyte plasma membrane.[18] Because of its small size, a single tolaasin molecule could not be responsible for the formation of an ion channel across the membrane, so probably channels are consti-

TABLE II. Average ϕ and ψ Angle Values and Angular Order Parameters for the 10 Periodically Sampled Structures of Tolaasin Along the Last 500 ps of rMD

Residue		Angle value		Angular order parameters
1	ΔBut	PHI	−77.8 ± 18.8	0.952
1	ΔBut	PSI	−39.2 ± 11.8	0.981
2	DPRO	PHI	67.5 ± 5.8	0.991
2	DPRO	PSI	23.8 ± 8.2	0.995
3	DSER	PHI	68.2 ± 7.1	0.993
3	DSER	PSI	27.8 ± 4.8	0.997
4	DLEU	PHI	82.3 ± 5.8	0.995
4	DLEU	PSI	40.3 ± 5.6	0.996
5	DVAL	PHI	59.2 ± 5.8	0.995
5	DVAL	PSI	41.4 ± 8.3	0.991
6	DSER	PHI	64.8 ± 9.8	0.987
6	DSER	PSI	37.3 ± 8.0	0.991
7	DLEU	PHI	70.6 ± 6.0	0.995
7	DLEU	PSI	56.0 ± 8.6	0.990
8	DVAL	PHI	52.9 ± 5.4	0.996
8	DVAL	PSI	43.1 ± 7.1	0.993
9	LVAL	PHI	43.0 ± 4.8	0.997
9	LVAL	PSI	56.1 ± 8.7	0.990
10	DGLN	PHI	66.5 ± 6.5	0.994
10	DGLN	PSI	24.7 ± 6.1	0.995
11	LLEU	PHI	48.2 ± 5.2	0.996
11	LLEU	PSI	41.9 ± 7.7	0.992
12	DVAL	PHI	82.4 ± 7.4	0.992
12	DVAL	PSI	37.1 ± 7.5	0.992
13	ΔBut	PHI	59.5 ± 9.2	0.989
13	ΔBut	PSI	21.8 ± 8.0	0.991
14	DalloTHR	PHI	93.4 ± 11.7	0.981
14	DalloTHR	PSI	37.9 ± 10.6	0.985
15	LILE	PHI	−53.0 ± 7.6	0.992
15	LILE	PSI	−37.9 ± 5.4	0.996
16	LHSE	PHI	−86.1 ± 8.0	0.991
16	LHSE	PSI	2.0 ± 9.8	0.987
17	DDAB	PHI	92.4 ± 10.8	0.984
17	DDAB	PSI	−28.8 ± 14.8	0.970
18	LLYS	PHI	−84.6 ± 18.1	0.956

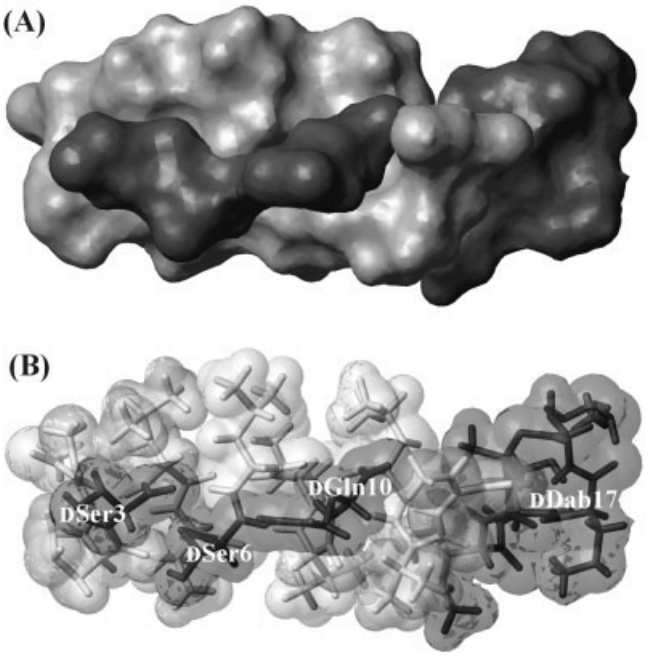

Fig. 5. Representation of van der Waals surfaces of tolaasin. **A:** Hydrophilic and hydrophobic residues are depicted in black and gray, respectively. **B:** van der Waals surfaces spread over a stick representation of tolaasin. Hydrophilic residues are labeled along the chain, including the lactone ring.

tuted by aggregation of amphipathic α-helical monomers. Zn^{2+} was able to inactivate ion channels, probably via chelation of ionizable groups in the membrane near the site of the pore formation.[14] The normal eukaryotic cells such as erythrocytes predominantly express the zwitterionic phospholipid phosphatidylcholine on their outer leaflet. On the contrary, the surface of bacteria contains lipopolysaccharides (in Gram-negative bacteria) and polysaccharides (teichoic acids, in Gram-positive bacteria), and their inner membranes contain phosphatidylglycerol, all of which are negatively charged. Our tolaasin secondary structure suggests that the amphipathic N-terminal α-helix might be deeply anchored into the membrane, leaving the hydrophilic charged lactone ring close to the surface of membrane. A longer anchored tail might both result in a higher affinity to the membrane and a stronger disrupting effect through the whole thickness of the membrane. Moreover, the length of the N-terminal sequence might play a central role in the formation of stable oligomeric structures required to cause ion channel formation. This might explain the loss of activity in ion channels formation observed in the case of tolaasin 144 (an altered toxin lacking DSer6-DLeu7-DVal8) to form ion channels in lipid bilayers and to lyse erythrocytes at wild-type effective tolaasin concentrations. Preliminary MD simulations indicate that the N-terminal sequence of tolaasin 144 is more flexible than wild-type tolaasin and does not fold into a stable α-helix, most likely preventing the formation of oligomeric aggregates. This structural finding agrees with the fact that tolaasin lyses erythrocytes by two mechanisms.[53] The first one is observed at low concentrations of tolaasin and is the result of Zn^{2+}-sensitive ion channel formation. The second mechanism is observed at high concentrations of both tolaasin and tolaasin 144, and is the result of Zn^{2+}-insensitive detergent action of both molecules.

It has been reported that the α-helical structure, while important for cytotoxicity toward mammalian cells, is not a prerequisite for antibacterial activity.[7] Novel antibiotic peptides useful as therapeutic drugs require strong antibiotic activity against bacterial and fungal cells without hemolytic effect. Functional and structural studies with D-amino acids incorporated analogues of pardaxin reveal that the lack of a significant α-helix does not prevent the lysis of bacterial membrane, the peptide probably acting as a detergent in what has been described as a "carpet"-like mechanism.[4,7] Therefore, the decrease of the helical content into lytyc peptides by incorporating D-amino acids may be a useful approach to discover new peptide antibiotics for therapeutic use. In this context, tolaasin and tolaasin 144 are very interesting molecules: the presence

of a stable α-helix in the former warrants its lytyc activity, while the decreased helical content together with the detergent action exerted by tolaasin 144 strongly suggest its possible role as antibacterial, but not cytotoxic, peptide. Furthermore, they naturally present L- amino acids into a D- amino acid sequence: this induces resistance to enzymatic degradation and inactivation,[5] and increase antigenicity.[6]

The antimicrobial activity of tolaasin reported in this review, though limited to a representative set of test micro-organisms, confirmed the high sensitivity of Gram-positive bacteria as previously reported,[18] and showed a quite good activity of tolaasin toward the yeast *R. pilimanae* and the Gram-negative bacterium *E. coli*. The activity against *E. coli* (strain ITM100), in contrast with the results reported,[18] indicates a variability of sensitivity among strains, and strongly suggests that before conclusions are drawn, several strains of the same microorganisms must be checked. It would be of interest to test tolaasin and tolaasin 144 against Gram-positive *Bacillus subtilis* and *Staphylococcus aureus*, and against Gram-negative *Streptococcus pneumonieae* and vancomycin-resistant *Enterococcus faecalis*.

Finally, the structural information on tolaasin can be extremely helpful for its possible use in the control of the brown blotch disease of *A. bisporus* also in combination with other methods. Treatment of mushrooms caps with tolaasin provokes pitting and browning[18,47] as well as activation of the defense mechanism of the mushroom.[54] Nutkins et al.[13] reported that partially purified toxin reproduces disease symptoms, as does the intact organism, although tolaasin induces more prominent symptoms than living bacteria.[55] Accordingly, tolaasin appears to be an adequate target to stop the sequence of events affecting *A. bisporus*. The fact that white line inducing principle (WLIP, a lipodepsipeptide produced by *Pseudomonas "reactans"* and responsible for a specific interaction with tolaasin in the "white line test"[26]) appears to be able to inhibit the browning[50] could confirm this hypothesis.

Structural studies on the tolaasin-WLIP interaction are in progress in our laboratory.

ACKNOWLEDGMENTS

F.J. was a TMR post-doctoral fellow supported by the European Union under contract ERBFMRXCT960069.

REFERENCES

1. Segrest JP, DeLoof H, Dohlman JG, Brouillette CG, Anantharamaiah GM. Amphipathic helix motif: classes and properties. Proteins 1990;8:103–117.
2. Westerhoff HV, Juretic D, Hendler RW, Zasloff M. Magainins and the disruption of membrane-linked free-energy transduction. Proc Natl Acad Sci USA 1989;87:6597–6601.
3. Ojcius DM, Young JDE. Cytolytic pore-forming proteins and peptides: is there a common structural motif? Trends Biochem Sci 1991;16:225–229.
4. Shai Y. Molecular recognition between membrane-spanning polypeptides. Trends Biochem Sci 1995;20:460–464.
5. Wade D, Boman A, Wåhlin B, Andreu D, Boman HG, Merrifield RB. All-D amino acid-containing channel-forming antibiotic peptides. Proc Natl Acad Sci USA 1990;87:4761–4765.
6. Benkirane N, Friede M, Guichard G, Briand JP, Van RM, Muller S. Antigenicity and immunogenicity of modified synthetic peptides containing D- amino acid residues. Antibodies to a D- enantiomer do recognise the parent L-hexapeptide and reciprocally. J Biol Chem 1993;268:26279–26285.
7. Shai Y, Oren Z. Diastereoisomers of cytolysins, a novel class of potent antibacterial peptides. J Biol Chem 1996;271:7305–7308.
8. Oren Z, Shai Y. Selective lysis of bacteria but not mammalian cells by diastereomers of melittin: structure-function study. Biochemistry 1997;36:1826–1835.
9. Bender CL, Alarcón-Chaidez F, Gross DC. *Pseudomonas syringae* phytotoxins: mode of action, regulation, and biosynthesis by peptide and polyketide synthetases. Microbiol Mol Biol Rev 1999; 63:266–292.
10. Ballio A, Barra D, Bossa F, Collina A, Grgurina I, Marino G, Moneti G, Paci M, Pucci P, Segre A, Simmaco M. Syringopeptins, new phytotoxic lipodepsipeptides of *Pseudomonas syringae* pv. *syringae*. FEBS Lett 1991;291:109–112.
11. Raney PB, Brodey CL, Johnstone K. Biology of *Pseudomonas tolaasii*, cause of brown blotch disease of the cultivated mushroom. Adv Plant Pathol 1992;8:95–117.
12. Tolaas AG. A bacterial disease of cultivated mushroom. Phytopathology 1915;5:51–54.
13. Nutkins JC, Mortishire-Smith RJ, PackmanLC, Brodey CL, Rainey PB, Johnstone K, Williams DH. Structure determination of tolaasin, an extracellular lipodepsipeptide produced by the mushroom pathogen *Pseudomonas tolaasii* Paine. J Am Chem Soc 1991;113: 2621–2627.
14. Brodey CL, Rainey PB, Tester M, Johnstone K. Bacterial blotch disease of the cultivated mushroom is caused by an ion-channel forming lipodepsipeptide toxin. Mol Plant Microbe Interact 1991; 4:407–411.
15. Fox RO, Richards FM. A voltage-gated ion channel model inferred from the crystal structure of alamethicin at 1.5-Å resolution. Nature 1982;300:325–330.
16. Sansom MSP. Structure and function of channel-forming peptaibols. Q Rev Biophys 1993;26:365–421.
17. Cafiso DS. Alamethicin: a peptide model for voltage gating and protein-membrane interactions. Ann Rev Biophys Biomol Struct 1994;23:141–165.
18. Raney PB, Brodey CL, Johnstone K. Biological properties and spectrum of activity of tolaasin, a lipodepsipeptide toxin produced by the mushroom pathogen *Pseudomonas tolaasii*. Physiol Mol Plant Pathol 1991;39:57–70.
19. DeGrado WF, Wasserman ZR, Lear JD. Protein design, a minimalist approach. Science 1989;243:622–628.
20. Bechinger B, Zasloff M, Opella SJ. Structure and orientation of the antibiotic peptide magainin in membranes by solid-state nuclear magnetic resonance spectroscopy. Protein Sci 1993;2:2077–2084.
21. Scwhyzer R. Molecular mechanism of opioid receptor selection. Biochemistry 1986;25:6335–6342.
22. Mortishire-Smith RJ, Drake AF, Nutkins JC, Williams DH. Left handed alpha-helix formation by a bacterial peptide. FEBS Lett 1991;278:244–246.
23. King EO, Ward MK, Raney DE. Two simple media for the demonstration of pyocyanin and fluorescein. J Lab Clin Med 1954;44:301–307.
24. Iacobellis NS, Lavermicocca P, Grgurina I, Simmaco M, Ballio A. Phytotoxic properties of *Pseudomonas syringae* pv. *Syringae toxins*. Physiol Mol Plant Pathol 1992;40:107–116.
25. Lavermicocca P, Iacobellis NS, Simmaco M, Graniti A. Biological properties and spectrum of activity of *Pseudomonas syringae* pv. *syringae* toxins. Physiol Mol Plant Pathol 1997;50:129–140.
26. Peng JT. Resistance to disease in *A. bisporus* (Lange) Imbach. Ph.D. Thesis, University of Leeds, Department of Plant Science; 1996.
27. Jeener J, Meier BH, Bachmann P, Ernst RR. Investigation of exchange processes by two-dimensional NMR spectroscopy. J Chem Phys 1976;71:4546–4553.
28. Braunschweiler L., Ernst RR. Coherence transfer by isotropic mixing: application of proton correlation spectroscopy. J Magn Reson 1983;53:521–528.
29. Drobny G, Pines A, Sinton S, Weitkamp D, Wemmer D. Fourier transform multiple quantum nuclear magnetic resonance. Faraday Div Chem Soc Symp 1979;13:49–55.
30. Piotto M, Saudek V, Sklenar V. Gradient-tailored excitation for single-quantum NMR spectroscopy of aqueous solutions. J Biomol NMR 1992;2:661–666.

31. Griesinger C, Otting G, Wüthrich K, Ernst RR. Clean TOCSY for 1H spin system identification in macromolecules. J Am Chem Soc 1988;110:7870–7872.
32. Bax A, Davis DG. MLEV-17-based two-dimensional homonuclear magnetisation transfer spectroscopy. J Magn Reson 1985;65:355–366.
33. Pearlman DA, Case DA, Caldwell JW, Ross WS, Cheatman III TE, DeBolt S, Ferguson D, Seibel G, Kollman P. AMBER, a package of computer programs for applying molecular mechanics, normal mode analysis, molecular dynamics and free energy calculations to simulate the structural and energetic properties of molecules. Comp Phys Commun 1995;91:1–41.
34. Wüthrich K, Billeter M, Braun W. Pseudo-structures for the 20 common amino acids for use in studies of protein conformations by measurements of intramolecular proton-proton distance constraints with nuclear magnetic resonance. J Mol Biol 1983;169: 949–961.
35. Wüthrich K. NMR in proteins and nucleic acids. New York: John Wiley & Sons; 1986.
36. Weiner SJ, Kollman PA, Case DA, Singh UC, Ghio C, Alagona G, Profeta S Jr, Weiner PA. A new force field for molecular mechanical simulation of nucleic acids and proteins. J Am Chem Soc 1981;106:765–784.
37. Weiner PK, Kollman PA, Nguyen DT, Case DA. An all-atom force-field for molecular mechanical simulation of nucleic acids and proteins. J Comput Chem 1986;7:230–252.
38. Berendsen HJC, Postma JPM, van Gunsteren WF, Di Nola A, Haak JM. Molecular dynamics with coupling to an external bath. J Chem Phys 1984;81:3684–3690.
39. Ryckaert JP, Ciccotti G, Berendsen HJC. Numerical integration of the Cartesian equations of motions of a system with constraints: molecular dynamics of n-alcanes. J Comp Phys 1977;23:327–341.
40. Case DA, Pearlman DA, Caldwell JW, Cheatham III TE, Wang J, Ross, WS, Simmerling CL, Darden TA, Merz KM, Stanton RV, Cheng AL, Vicent JJ, Crowley M, Tsui V, Gohlke H., Radmer RJ, Duan Y, Pitera J, Massova I, Seibel GL, Singh UC, Weiner PK, Kollman PA. AMBER 7, University of California, San Francisco. 2002.
41. Darden T, York D, Pedersen L. Particle mesh Ewald- -an Nlog(N) method for Ewald sums in large systems. J Chem Phys 1993;98: 10089–10092.
42. Essmann U, Perera L, Berkowitz ML, Darden T, Lee H, Pedersen LG. A smooth particle mesh Ewald method. J Chem Phys 1995;103: 8577–8593.
43. Tsui V, Case DA. Molecular dynamics simulations of nucleic acids with a generalized Born Solvation model. J Am Chem Soc 2000;122:2489–2498.
44. Koradi R, Billeter M, Wüthrich K. MOLMOL: a program for display and analysis of macromolecular structures. J Mol Graph 1996;14:51–55.
45. Wagner G, Neuhaus D, Wörgötter E, Vasák M, Kägi JRH, Wüthrich K. Nuclear magnetic resonance identification of "half-turn" and 3(10)-helix secondary structure in rabbit liver metallothionein-2. J Mol Biol 1986;187:131–135.
46. Dyson HJ, Rance M, Houghten RA, Wright PE, Lerner RA. Folding of immunogenic peptide fragments of proteins in water solution. II. The nascent helix. J Mol Biol 1988;201:201–217.
47. Ballio A, Bossa F, Di Giorgio A, Di Nola C, Manetti M, Paci M, Scaloni A, Segre A. Solution conformation of the *Pseudomonas syringae pv. syringae* phytotoxic lipodepsipeptide syringopeptin 25-A. Two-dimensional NMR, distance geometry and molecular dynamics. Eur J Biochem 1995;234;747–758.
48. Storm DR, Rosenthal KS, Swanson PE. Polymyxin and related peptide antibiotics. Annu Rev Biochem 1977;46:723–763.
49. Clark DP, Durell S, Maloy W, Zasloff M. Ranalexin. A novel antimicrobial peptide from bullfrog (*Rana catesbeiana*) skin, structurally related to the bacterial antibiotic, polymyxin. J Biol Chem 1994;269:10849–10855.
50. Simmaco M, Mignogna G, Barra D, Bossa F. Antimicrobial peptides from skin secretions of *Rana esculenta*. Molecular cloning of cDNAs encoding esculentin and brevinins and isolation of new active peptides. J Biol Chem 1994;269:11956–11961.
51. Oren Z, Shai Y. Mode of action of linear amphipathic alpha-helical antimicrobial peptides. Biopolymers 1998;47:451–463.
52. Andreu D, Rivas L. Animal antimicrobial peptides: an overview. Biopolymers 1998;47:415–433.
53. Hutchison ML, Johnstone K. Evidence for the involvement of the surface active properties of the extracellular toxin tolaasin in the manifestation of brown blotch disease symptoms by *Pseudomonas tolaasii* on *Agarus bisporus*. Physiol Mol Plant Pathol 1993;42:373–384.
54. Soler-Rivas C, Jolivet S, Arpin N, Oliver JM, Wichers HJ. Biochemical and physiological aspects of brown blotch disease of *Agaricus bisporus*. FEMS Microbiol Rev 1999;23:591–614.
55. Moquet F, Mamoun M, Olivier JM. *Pseudomonas tolaasii* and tolaasin: comparison of symptom induction on a wide range of *Agaricus bisporus* strains. FEMS Microbiol Lett 1996;142:99–103.